

Zhenguo Wang, Charles Reisman, Jonathan Liu,  
and Kinpui Chan

Optical coherence tomography (OCT), first introduced in 1991, is an enabling optical, noninvasive imaging modality that provides cross-sectional visualization of biological tissues with resolutions one to two orders of magnitude better than conventional ultrasound [1]. Because the eye is optically accessible for visible and near-infrared light, ophthalmic OCT has been the most successful clinical application from the invention of OCT with an unparalleled combination of axial resolution (1–10  $\mu\text{m}$ ) and penetration depth (1–2 mm in tissue). This chapter presents a brief introduction of OCT, including the early time-domain OCT (TD-OCT) and the more recent Fourier-domain OCT (FD-OCT), which can be characterized into the two forms of spectral-domain OCT (SD-OCT) and swept source OCT (SS-OCT). Since the commercial launch of SD-OCT in 2006 by multiple manufacturers, including the world's first Topcon 3D OCT-1000, the significant practical advantages of both higher speed and higher sensitivity of SD-OCT over TD-OCT [2–4] have led to a widespread use of OCT instruments in ophthalmology [5]. On the other hand, SS-OCT, which employs the state-of-the-art high-speed wavelength tuning laser (swept source) as well as digital data acquisition and processing technology, offers further advantages of overcoming the signal roll-off observed for SD-OCT at a deeper range along with an unprecedented A-scan rate for wider field-of-view structural OCT and OCT angiography imaging [6, 7]. With advances in commercial wavelength tuning lasers, the first clinical 1  $\mu\text{m}$  SS-OCT machine, Topcon DRI OCT-1 Atlantis, became commercially available for retinal imaging in 2012 [8].

As shown in Fig. 1.1, OCT measures the optical backscattering profile (intensity and time of flight of backscattered light) along the axial direction (A-scan), analogous to measuring echoes of sound waves in conventional ultrasound imaging. A two-dimensional cross-sectional image (B-scan)

is produced by transversely scanning the incident optical beam and performing sequential A-scans. Similarly, volumetric data sets can be generated by acquiring sequential B-scans along the transverse direction.

Since the speed of light is much higher than that of sound waves, it is very challenging, if not impossible, to directly measure the time of flight for backscattered light. Instead, OCT is based on low coherence interferometry to measure the time of flight indirectly from optical interference generated by mixing the backscattered light with light from a reference mirror. A Michelson interferometer is most commonly employed in OCT systems. Light from the broadband light source is divided by a beam splitter into the reference and sample arms. The reflected light from these two arms are recombined again through the beam splitter and detected with a photodetector. Depending on the method used to reconstruct the intensity and time of flight of backscattered light, there are two types of OCT techniques, namely TD-OCT and FD-OCT.

In a TD-OCT system, a moving mirror is placed in the reference arm, and a single photodetector is employed. As the reference mirror in an OCT system moves along the axial direction, a corresponding depth-dependent backscattering profile of the sample is acquired. The axial resolution of OCT is determined by the coherence length of the light source, while the imaging speed is determined by how fast the reference mirror moves. Due to the relatively slow speed of the mechanical reference mirror, the imaging speed of commercial ophthalmic TD-OCT has been limited to 400 A-scans per second [9].

To further increase the imaging speed and the sensitivity, SD-OCT based on a fast linear detector array was demonstrated for retinal imaging in vivo in the early 2000s [10]. In a SD-OCT system, the reference mirror is stationary instead of moving. The imaging speed is determined by the speed of the linear detector array, which can be higher than tens of thousands of A-scans per second [11], yielding a roughly 100 $\times$  improvement over that achieved with TD-OCT

---

Z. Wang, PhD (✉) • C. Reisman • J. Liu • K. Chan  
Topcon Advanced Biomedical Imaging Laboratory,  
Oakland, NJ, USA  
e-mail: [zwang@topcon.com](mailto:zwang@topcon.com)

systems. SD-OCT detects the interferogram as a function of wavelength ( $\lambda$ ), in contrast to the direct detection of back-scattering profile as a function of depth position of the reference mirror in TD-OCT. As illustrated in Fig. 1.2, the depth information, more precisely the depth difference between the reference mirror and the sample, is encoded as the frequency of the interferogram fringes. When the depth of the sample is near to that of the reference mirror, the frequency of interferogram fringes is low (Fig. 1.2a). And when the depth of the sample is far from that of the reference mirror, the frequency of interferogram fringes is high (Fig. 1.2b). Light backscattered from different depths along the axial direction are detected simultaneously using a linear detector array (Fig. 1.2c). By performing a Fourier transform on the detected interferogram in wavenumber ( $k$ ), an A-scan profile can be readily acquired.

The higher speed and sensitivity of SD-OCT [2–4] has enabled volumetric imaging with better image quality. On the other hand, SD-OCT is subject to a signal-to-noise ratio (SNR) roll-off characteristic that occurs in the FD-OCT technique. As shown in Fig. 1.3, it is commonly observed in SD-OCT that the reconstructed sample signal intensity gets weaker when it is farther from the zero-delay position.

This SNR roll-off is primarily caused by the limited capability of SD-OCT to resolve the interferogram fringes. In an SD-OCT system using a broadband light source such as a superluminescent diode (SLD), the interferogram is generated by the spectrometer in the detection arm, which spreads the light at different wavelengths to be recorded by a linear detector array. However, due to the finite number of pixels on the linear detector array, the light of different wavelengths that are very close to each other fall on the same pixel and gets digitized without distinction, as illustrated in Fig. 1.4.

As a consequence, the resolvability of interferogram fringes is degraded. Mathematically, this constitutes an integration effect of the interferogram over the continuous spectrum of the light source across each element of the linear detector array. In other words, the resolvability of the interferogram fringes is affected differently during detection depending on frequency. As shown in Fig. 1.3, the higher the fringe frequency is, the more it is attenuated and the weaker its amplitude becomes. Accordingly, after Fourier transform, the amplitude of the reconstructed signal will be depth dependent. It was reported that the SNR roll-off for SD-OCT can be as high as 15 dB/mm [12]. Considering the typical 2 mm imaging range for commercial ophthalmic OCT instrument, an SNR drop of up to 30 dB is very significant and it is not unusual that the lower end of the imaging range is practically unusable.

By eliminating the use of the spectrometer and the linear detector array, SS-OCT employs a rapid-wavelength tuning

laser and high-speed photodetector and signal digitizer. SS-OCT thereby offers a significant solution to the limitation of spectrometer spectral resolution as seen in SD-OCT, and thus enables deeper range imaging without compromising the sensitivity at a deeper position caused by the above-mentioned SNR roll-off. As illustrated in Fig. 1.5, the instantaneous line width of the laser light source used in SS-OCT, rather than the finite pixel size of the linear detector array used in SD-OCT, primarily determines the resolvability of the interferogram fringes.

The instantaneous line width characterizes how pure the laser mode is at one particular moment while it is swept through a range of individual wavelengths. Ideally, the tuning laser is emitting light at a single wavelength at any given moment. In reality, the emitted light is typically composed of photons of more than one wavelength spanning across a certain range that is characterized as instantaneous line width. Such wavelength impurity affects the interferogram similarly as finite pixel size of linear detector array in SD-OCT and causes SNR roll-off as well. However, with the recent advances in laser technology, the commercial tuning lasers have dramatically improved instantaneous line width [12]. Therefore, the interferogram fringes can be well-resolved across the entire imaging range. The SNR roll-off in SS-OCT systems enabled by the latest vertical-cavity surface emitting lasers (VCSEL) is virtually zero within the imaging range of up to 50 mm [13].

In addition, SS-OCT is able to operate in the 1  $\mu\text{m}$  wavelength range. Besides low water absorption and minimal depth-dependent dispersion [14], 1  $\mu\text{m}$  wavelength OCT is less susceptible to scattering in tissue such as cataract and hemorrhage [15]. It can also better penetrate the retina pigment epithelium (RPE) and visualize deeper structures in the choroid layer and sclera [16, 17]. The practical benefits of 1  $\mu\text{m}$  wavelength SS-OCT can be appreciated by comparing retinal images at different depths acquired with an 800 nm wavelength SD-OCT system (Topcon 3D OCT-2000) and a 1  $\mu\text{m}$  wavelength SS-OCT system (Topcon DRI-OCT Triton), as shown in Fig. 1.6.

The capability to obtain images with high quality at any depth within the imaging range not only makes it easier for patients and medical practitioners to take OCT images, but also facilitates a large imaging range that is able to accommodate the curvature of eyeball. More importantly, 1  $\mu\text{m}$  wavelength SS-OCT enhances visualization of previously obscured features together with the retina in the same image without sophisticated imaging processing, as shown in Fig. 1.7.

This has helped choroidal imaging, posterior vitreous visualization [18], and ophthalmic research in new frontiers [19–22]. The recent development of OCT angiography based on 1  $\mu\text{m}$  wavelength SS-OCT also demonstrated functional imaging ability by visualizing the choriocapillaris and

choroidal microvasculature *in vivo* in normal human subjects [23].

The development of SS-OCT technology has enabled many attributes for a better clinical ophthalmic imaging instrument, including higher speed [6, 7, 12, 13], deeper imaging range with uniform sensitivity, reduced fringe wash-out [24], less light-scattering by cataract tissue, deeper penetration for better visualization of choroid and beyond [16, 25], invisibility of the scanning light for less distraction to patients during imaging, fewer motion artifacts, and potential for eventual miniaturization and cost-reduction [26]. Commercial SS-OCT development results were first presented by Topcon at ARVO 2010 [27]. Prototype Topcon

SS-OCT instruments for clinical research soon followed [28, 29]. Topcon continues to lead in clinical SS-OCT technology with the latest generation DRI-OCT Triton, which incorporates color fundus photography, fluorescein angiography, and fundus autofluorescence imaging, together with combined anterior and posterior eye OCT as well as OCT angiography. Cutting-edge SS-OCT technology opens the possibility for a new generation of multimodal ophthalmic instruments to image the entire eye, measure axial eye length [13], and acquire intraoperative OCT [30]. While SD-OCT is currently still dominant in the ophthalmic market, SS-OCT is expected to continue to grow and increasingly contribute to the medical community in the near future.

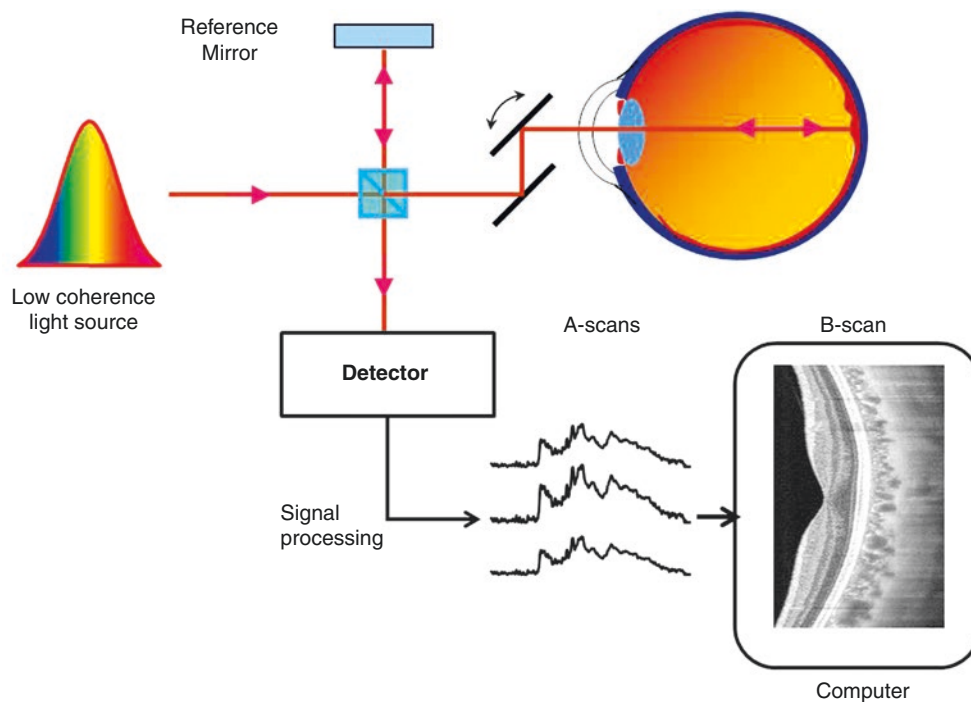


**Fig. 1.1** Schematic of an OCT system based on low coherence interferometry using a Michelson interferometer design. Light from a broadband light source is divided by a beam splitter into the reference and sample arms. The reflected light from these two arms are recombined again through the beam splitter and detected with a photodetector. OCT images are produced by scanning the light in the sample arm to acquire

sequential optical backscattering profiles along the axial direction. There are two types of OCT techniques, time-domain OCT (TD-OCT) and Fourier-domain OCT (FD-OCT), to reconstruct the intensity and time of flight of the backscattered light. In contrast to TD-OCT which uses a moving mirror in the reference arm, the reference mirror is stationary in FD-OCT, which includes spectral domain OCT and swept source OCT

**Fig. 1.2** Illustration of FD-OCT signal reconstruction. A-scans are generated by Fourier transforming the interferograms. (a) A low-frequency interferogram corresponds to a signal near the reference mirror. (b) A high-frequency interferogram corresponds to a signal far from the reference mirror. (c) OCT interferograms can have multiple frequency components comprised of signal from different depths as reconstructed in the A-scan profile

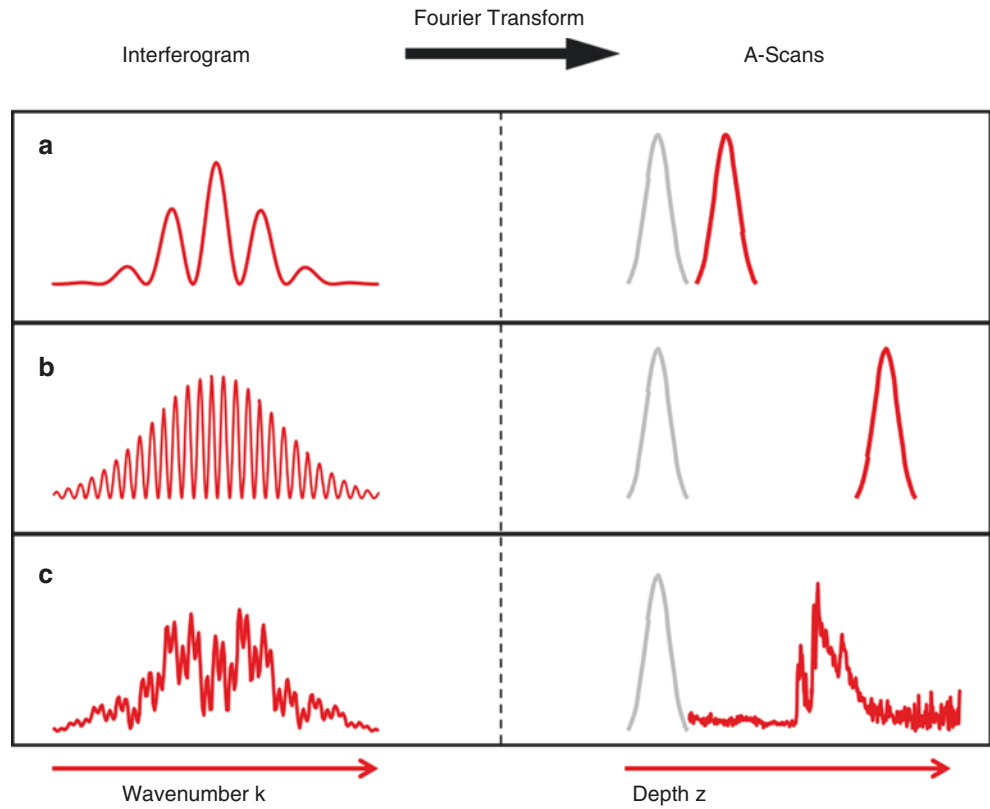


**Fig. 1.3** Illustration of signal roll-off in SD-OCT. The spectral resolution of the interferograms is limited by the spectrometer linear detector array. Higher frequency interferograms suffer more signal attenuation. The amplitude of reconstructed A-scans is therefore depth-dependent in SD-OCT

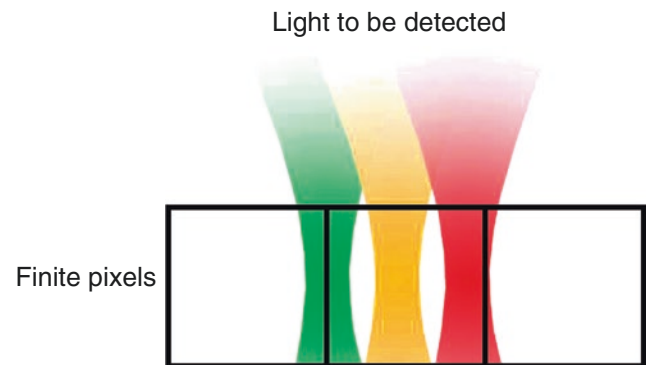
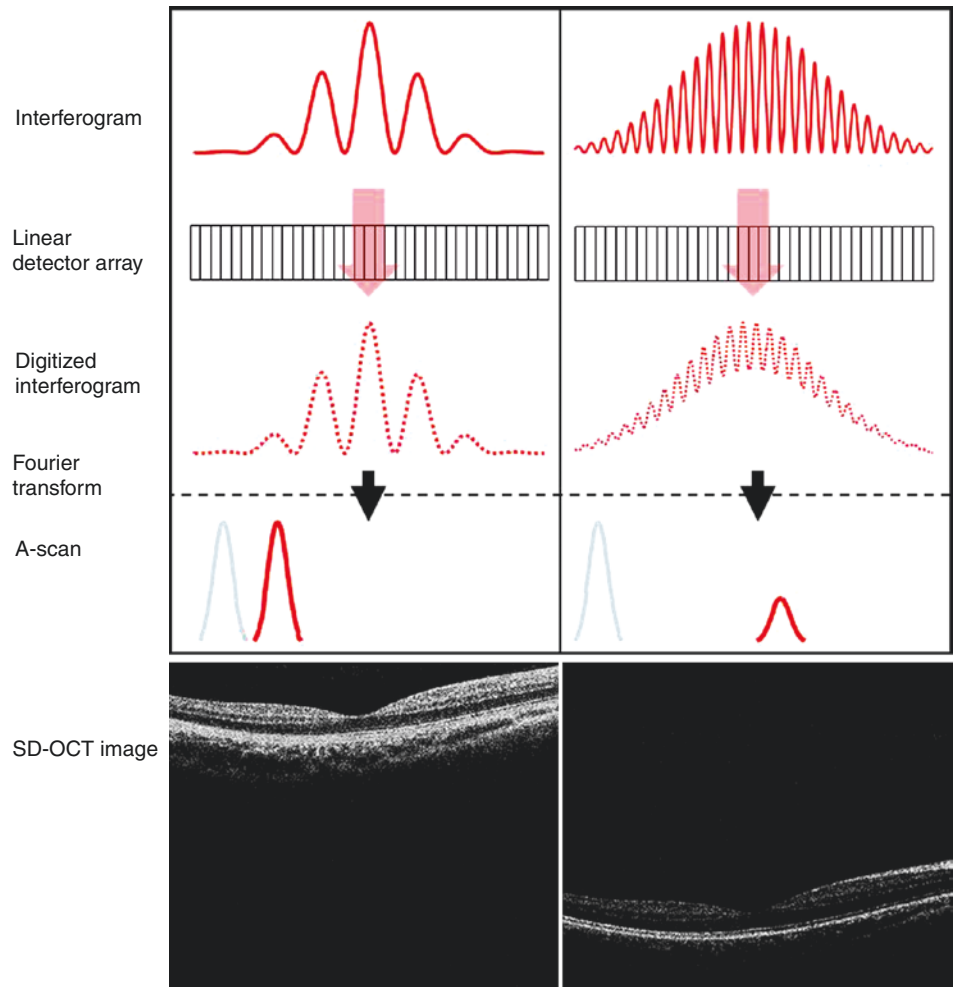


**Fig. 1.4** Illustration of the limitation in resolvability of different wave-length light on finite pixels in a spectral domain OCT spectrometer

**Fig. 1.5** Illustration of signal roll-off in SS-OCT. The tuning laser instantaneous line width and high-speed digitizer yields good resolvability of the interferograms. Higher frequency interferograms are well resolved without attenuation. The reconstructed A-scans therefore do not suffer from signal roll-off across the imaging range

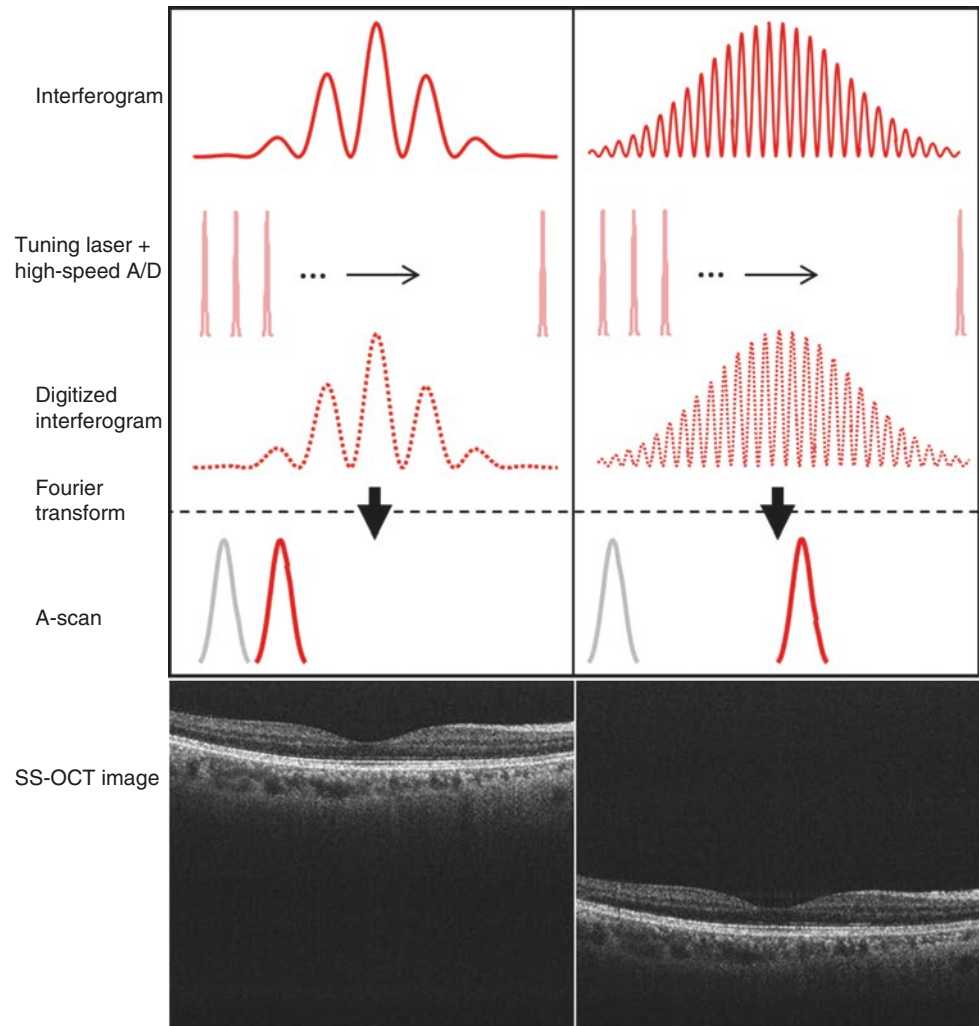




**Fig. 1.6** Retinal images at different depths acquired with 800 nm wavelength SD-OCT and 1  $\mu\text{m}$  wavelength SS-OCT. 1  $\mu\text{m}$  wavelength SS-OCT not only can visualize deeper structures in the choroid and sclera, but is also capable of obtaining high-quality images at any depth within the imaging range

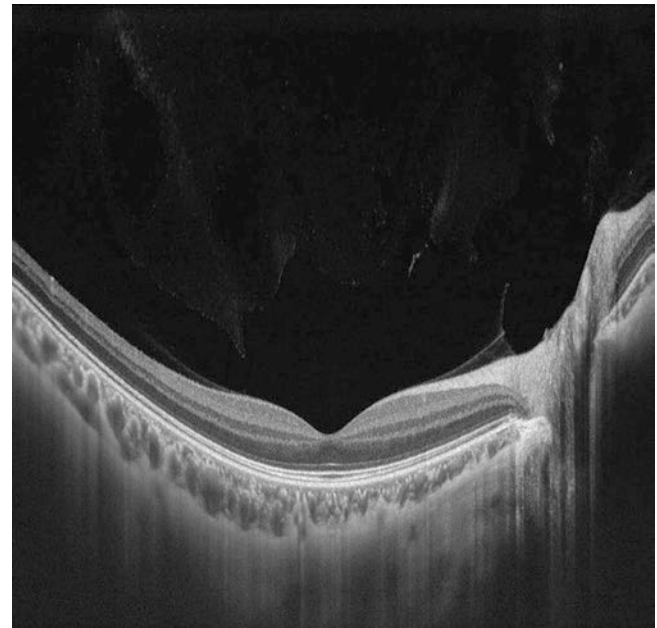
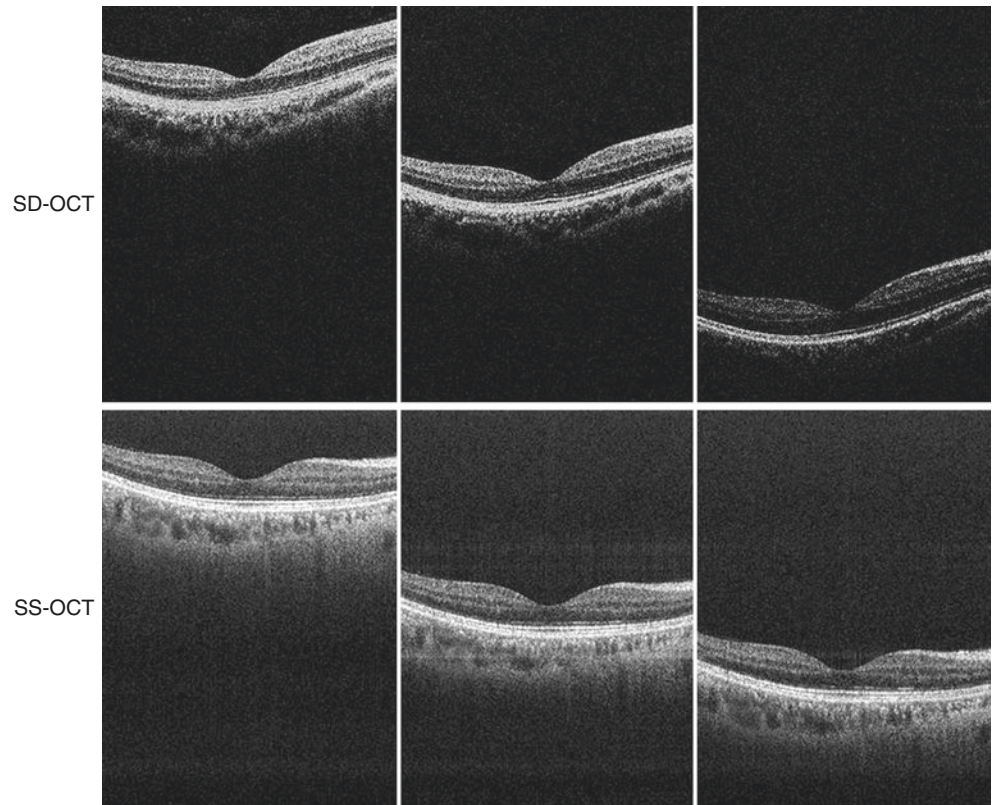


**Fig. 1.7** 1  $\mu\text{m}$  wavelength SS-OCT enhances visualization of previously obscured features together with the retina in the same image without sophisticated imaging processing. The visibility of fine details in the vitreous, choroid, and sclera are enabled by 1  $\mu\text{m}$  wavelength SS-OCT

## References

- Huang D, Swanson EA, Lin CP, Schuman JS, Stinson WG, Chang W, et al. Optical coherence tomography. *Science*. 1991;254(5035):1178–81.
- Leitgeb R, Hitzinger C, Fercher A. Performance of Fourier domain vs. time domain optical coherence tomography. *Opt Express*. 2003;11(8):889–94.
- De Boer JF, Cense B, Park BH, Pierce MC, Tearney GJ, Bouma BE. Improved signal-to-noise ratio in spectral-domain compared with time-domain optical coherence tomography. *Opt Lett*. 2003;28(21):2067–9.
- Choma M et al. Sensitivity advantage of swept source and Fourier domain optical coherence tomography. *Opt Express*. 2003;11(18):2183–9.
- Fujimoto J, Swanson E. The development, commercialization, and impact of optical coherence tomography. *Invest Ophthalmol Vis Sci*. 2016;57(9):OCT1–OCT13.
- Klein T, Wieser W, Eigenwillig CM, Biedermann BR, Huber R. Megahertz OCT for ultrawide-field retinal imaging with a 1050 nm Fourier domain mode-locked laser. *Opt Express*. 2011;19(4):3044–62.
- Klein T, Wieser W, Reznicek L, Neubauer A, Kampik A, Huber R. Multi-MHz retinal OCT. *Biomed Opt Express*. 2013;4(10):1890–908.
- AAO New Product Report. *Ophthalmology management*. 2012;16:60–6. <http://www.ophtalmologymanagement.com/articleviewer.aspx?articleID=107777>.
- Tearney GJ, Bouma BE, Fujimoto JG. High-speed phase- and group-delay scanning with a grating-based phase control delay line. *Opt Lett*. 1997;22(23):1811–3.
- Wojtkowski M, Leitgeb R, Kowalczyk A, Bajraszewski T, Fercher AF. In vivo human retinal imaging by Fourier domain optical coherence tomography. *J Biomed Opt*. 2002;7(3):457–63.
- Potsaid B, Gorczynska I, Srinivasan VJ, Chen Y, Jiang J, Cable A, et al. Ultrahigh speed spectral/Fourier domain OCT ophthalmic imaging at 70,000 to 312,500 axial scans per second. *Opt Express*. 2008;16(19):15149–69.
- Potsaid B, Baumann B, Huang D, Barry S, Cable AE, Schuman JS, et al. Ultrahigh speed 1050 nm swept source/Fourier domain OCT retinal and anterior segment imaging at 100,000 to 400,000 axial scans per second. *Opt Express*. 2010;18(19):20029–48.
- Grulkowski I, Liu JJ, Potsaid B, Jayaraman V, Lu CD, Jiang J, et al. Retinal, anterior segment and full eye imaging using ultrahigh speed swept source OCT with vertical-cavity surface emitting lasers. *Biomed Opt Express*. 2012;3(11):2733–51.
- Wang Y, Nelson J, Chen Z, Reiser B, Chuck R, Windeler R. Optimal wavelength for ultrahigh-resolution optical coherence tomography. *Opt Express*. 2003;11(12):1411–7.
- Esmaelpour M, Povazay B, Hermann B, Hofer B, Kacij V, Kapoor K, et al. Three-dimensional 1060-nm OCT: choroidal thickness maps in normal subjects and improved posterior segment visualization in cataract patients. *Invest Ophthalmol Vis Sci*. 2010;51(10):5260–6.
- Unterhuber A, Povazay B, Hermann B, Sattmann H, Chavez-Pirson A, Drexler W. In vivo retinal optical coherence tomography at 1040 nm-enhanced penetration into the choroid. *Opt Express*. 2005;13(9):3252–8.
- Huber R, Adler DC, Srinivasan VJ, Fujimoto JG. Fourier domain mode locking at 1050 nm for ultra-high-speed optical coherence tomography of the human retina at 236,000 axial scans per second. *Opt Lett*. 2007;32(14):2049–51.
- Spaide RF. Visualization of the posterior vitreous with dynamic focusing and windowed averaging swept source optical coherence tomography. *Am J Ophthalmol*. 2014;158(6):1267–74.
- Spaide RF, Akiba M, Ohno-Matsui K. Evaluation of peripapillary intrachoroidal cavitation with swept source and enhanced depth imaging optical coherence tomography. *Retina*. 2012;32(6):1037–44.
- Itakura H, Kishi S, Li D, Akiyama H. Observation of posterior pre-cortical vitreous pocket using swept-source optical coherence tomography. *Invest Ophthalmol Vis Sci*. 2013;54(5):3102–7.
- Stanga PE, Sala-Puigdollers A, Caputo S, Jaberansari H, Cien M, Gray J, et al. In vivo imaging of cortical vitreous using 1050-nm swept-source deep range imaging optical coherence tomography. *Am J Ophthalmol*. 2014;157(2):397–404.
- Flores-Moreno I, Arias-Barquet L, Rubio-Caso MJ, Ruiz-Moreno JM, Duker JS, Caminal JM. En face swept-source optical coherence tomography in neovascular age-related macular degeneration. *Br J Ophthalmol*. 2015;99(9):1260–7.
- Choi W, Mohler KJ, Potsaid B, Lu CD, Liu JJ, Jayaraman V, et al. Choriocapillaris and choroidal microvasculature imaging with ultrahigh speed OCT angiography. *PLoS One*. 2013;8(12):e81499.
- Hendargo HC, McNabb RP, Dhalla AH, Shepherd N, Izatt JA. Doppler velocity detection limitations in spectrometer-based versus swept-source optical coherence tomography. *Biomed Opt Express*. 2011;2(8):2175–88.
- Adhi M, Liu JJ, Qavi AH, Grulkowski I, Lu CD, Mohler KJ, et al. Choroidal analysis in healthy eyes using swept-source optical coherence tomography compared to spectral domain optical coherence tomography. *Am J Ophthalmol*. 2014;157(6):1272–81.
- Wang Z, Lee HC, Vermeulen D, Chen L, Nielsen T, Park SY, et al. Silicon photonic integrated circuit swept-source optical coherence tomography receiver with dual polarization, dual balanced, in-phase and quadrature detection. *Biomed Opt Express*. 2015;6(7):2562–74.
- Reisman CA, Yang Q, Wang Z, Tomidokoro A, Araie M, Hangai M, et al. Enhanced visualization and layer detection via averaging optical coherence tomography images. *Invest Ophthalmol Vis Sci*. 2010;51(13):3859. Presented at 2010 ARVO Annual Meeting.
- Hirata M, Tsujikawa A, Matsumoto A, Hangai M, Ooto S, Yamashiro K, et al. Macular choroidal thickness and volume in normal subjects measured by swept-source optical coherence tomography. *Invest Ophthalmol Vis Sci*. 2011;52(8):4971–8.
- Ohno-Matsui K, Akiba M, Moriyama M, Ishibashi T, Tokoro T, Spaide RF. Imaging retrolubar subarachnoid space around optic nerve by swept-source optical coherence tomography in eyes with pathologic myopia. *Invest Ophthalmol Vis Sci*. 2011;52(13):9644–50.
- Lu C, et al. Ultrahigh speed ophthalmic surgical OCT for intraoperative OCT angiography and widefield imaging. *Invest Ophthalmol Vis Sci*. 2016. Presented at 2016 ARVO Annual Meeting.